Available online at www.sciencedirect.com
ScienceDirect
Geochimica et Cosmochimica Acta 73 (2009) 4879–4890
Geochimica et Cosmochimica Acta
www.elsevier.com/locate/gca

The IIG iron meteorites: Probable formation in the IIAB core

John T. Wasson *, Won-Hie Choe [1]

Institute of Geophysics and Planetary Physics, University of California, Los Angeles, CA 90095-1567, USA

Received 29 January 2009; accepted in revised form 5 May 2009; available online 9 June 2009

Abstract

The addition of two meteorites to the iron meteorite grouplet originally known as the Bellsbank trio brings the population to five, the minimum number for group status. With Ga and Ge contents in the general "II" range, the new group has been designated IIG. The members of this group have low-Ni contents in the metal and large amounts of coarse schreibersite ($(Fe,NI)_3P$); their bulk P contents are 17–21 mg/g, the highest known in iron meteorites. Their S contents are exceptionally low, ranging from 0.2 to 2 mg/g. We report neutron-activation-analysis data for metal samples; the data generally show smooth trends on element-Au diagrams. The low Ir and high Au contents suggest formation during the late crystallization of a magma.

Because on element-Au or element-Ni diagrams the IIG fields of the important taxonomic elements Ni, Ga, Ge and As are offset from those of the IIAB irons, past researchers have concluded that the IIG irons could not have formed from the same magma, and thus that the two groups originated on separate parent bodies. However, on most element-Au diagrams the IIG fields plot close to extensions of IIAB trends to higher Au concentrations.

There is general agreement that immiscibility led to the formation of an upper S-rich and a lower P-rich magma in the IIAB core. We suggest that the IIG irons formed from the P-rich magma, and that schreibersite was a liquidus phase during the final stages of crystallization. The offsets in Ni and As (and possibly other elements) may result from solid-state elemental redistribution between metal and schreibersite during slow cooling. For example, it is well established that the equilibrium Ni content is >2× higher in late-formed relative to early-formed schreibersite. It is plausible that As substitutes nearly ideally for P in schreibersite at eutectic temperatures but becomes incompatible at low temperatures.

[Wasson J. T., Huber, H. and Malvin, D. J. (2007) Formation of IIAB iron meteorites. *Geochim. Cosmochim. Acta* **71**, 760–781] argued that, in the most evolved IIAB irons, the amount of trapped melt was high. The high P contents of IIG irons also require high contents of trapped melt but the local geometry seems to have allowed the S-rich immiscible melt to escape as it formed. The escaping melt may have selectively depleted elements such as Au and Ge.

1. INTRODUCTION

The meteorites Bellsbank, La Primitiva and Tombigbee River were recognized to have similar compositions and structures by Wasson and Kimberlin (1967). They were described in more detail by Scott et al. (1973). Their structures are marked by very high contents of coarse (skeletal, hieroglyphic) schreibersite (Buchwald, 1975). At some point in the 1970s the grouplet was given the designation the "Bellsbank Trio". Wasson (1974) proposed that five be considered the minimum number of meteorites required to form a group. With the addition of Twannberg and Guanaco the grouplet has become a group. Because the Ge and Ga contents are within the general range covered by Roman numeral II, this genetic set has been designated group IIG.

In 1984 the Twannberg iron was discovered in Switzerland, and shown to have a composition and structure closely similar to those of the Bellsbank trio irons; a first set of compositional data was published by Wasson et al.

* Corresponding author.
E-mail address: jtwasson@ucla.edu (J.T. Wasson).
[1] Dept. of Earth and Space Sciences and Dept. of Chemistry and Biochemistry Usern:a-W6372 Password 6SNWWN0.

0016-7037/$ - see front matter © 2009 Elsevier Ltd. All rights reserved.
doi:10.1016/j.gca.2009.05.062

(1989). Analyses of additional Twannberg specimens are provided in Hofmann et al. (2009). The Guanaco meteorite was discovered in Chile in 2000 (Russell et al., Meteoritical Bull. 88, 2004). Although La Primitiva is also from Chile, the discovery locations are separated by ~600 km and the meteorites were shown to have distinctive contents of Ir; we show below that resolvable differences are found in most elements. This is the first detailed compositional comparison of the members of the new group. We now also show that most compositional trends in these five meteorites are consistent with them being highly evolved products of the IIAB magma.

In addition to having exceptionally high concentrations of P, the group-IIG irons have very low concentrations of S. One possible way to produce a high-P, low-S magma is liquid immiscibility (Ulff-Møller, 1998; Chabot and Drake, 2000; Wasson and Huber, 2006), as seems to have occurred during the crystallization of the IIAB magma.

2. ANALYTICAL TECHNIQUES AND SAMPLES

With the exception of Twannberg (for which Wasson et al. (1989) and Hofmann et al. (2009) published data) this is the first report of INAA data for IIG irons. As shown in Table A1, most of the data were gathered between 2001 and 2008. To the degree possible we avoided schreibersite in our analyses, thus they represent metal rather than whole rock.

We currently determine up to 15 elements (14 plus Fe) in metal by instrumental neutron-activation analysis (INAA) in replicate analyses; data for Fe are used for internal normalization. Although we recently started to determine Ru routinely, we did not determine it in the INAA runs reported in this data set. All Ge data except those for Guanaco and the one Sb datum were determined by radiochemical neutron-activation analysis (RNAA); the 95% uncertainty in the Guanaco mean Ge value is about 10% relative. All Re values were below our detection limit of ~20 ng/g.

The meteorites were analyzed at least twice and several were analyzed additional times to improve the precision. The procedures are those given by Wasson et al. (1989) except for two minor changes. The mean thickness of the ca. 550-mg samples is now 3.0 instead of 3.2 mm, and we now apply small (generally in the range 0.95–1.05) sample-specific geometric corrections to make the Ni and Co values in the first count agree better with those from the third and fourth counts (which are corrected to make Fe + Ni = 990 mg/g). We then choose a correction factor for the second count that is intermediate between that for the first and the mean corrections in the third and fourth counts. Some additional details are found in the experimental section of Wasson et al. (2007).

We estimate relative 95% confidence limits on the listed means to be 1.5–3% for Co, Ga, and Au, 4–6% for Ni, As, Ir and (RNAA) Ge, 7–10% for W (values >0.3 μg/g), and Pt (>2 μg/g). All W and Pt values in IIG irons are below the listed limits; uncertainties are in the 15–30% range. Because much of the Cr is in minor phases, sampling errors result in relative confidence limits on the mean ⩾10%. In addition, there is an Fe interference in the determination of Cr resulting from the 54Fe (n,α) 51Cr fast-neutron reaction; our somewhat uncertain estimate of the level of interference is 6 μg Cr per g of Fe (Wasson and Richardson, 2001). Our data were not corrected for this interference.

Hofmann et al. (2009) listed our INAA data for Twannberg masses I and II; we now have data for Twannberg III and an additional replicate on Twannberg I. As discussed by Hofmann et al. (2009) and recognizable in the replicate data in Table A1, there appear to be resolvable compositional differences between Twannberg I and Twannberg II and III. However, the range is small compared to the total range in IIG.

The five meteorites listed in Tables 1 and A1 comprise the entire known set of IIG irons. The number of well characterized iron meteorites is ca. 740, thus the mean IIG abundance among irons is 0.7% (±0.3%).

3. RESULTS

3.1. Petrographic observations

The structure of the Bellsbank iron is illustrated in Fig. 1. All visible inclusions are schreibersite, and the dark hole on the upper left resulted from the loss of schreibersite. As discussed by various authors and in detailed fashion by Hofmann et al. (2009), the schreibersite in IIG irons is present in three forms: (1) the irregular coarse inclusions common on the right side of Fig. 1 are the most abundant; (2) long (several cm), narrow (5–20 μm) lamella, visible on the left side of this image, are relatively common; and, not visible in this photo, (3) tiny microschreibersites (commonly known as rhabdites) that have lengths of several (up to 10) μm and widths of 1–3 μm.

The UCLA Guanaco specimens are unpolished; they have a total surface area of about 200 cm^2 if one counts both sides of the relatively thin (ca. 7 mm) specimens. They

Table 1
Mean concentrations of 14 elements in five IIG iron meteorites; meteorites arranged in order of increasing Au content. All data obtained by INAA except Ge and Sb values (both RNAA) and P and S (modal analyses: see text for details).

	Cr μg/g	Co mg/g	Ni mg/g	Cu μg/g	Ga μg/g	Ge μg/g	As μg/g	Sb ng/g	W μg/g	Re ng/g	Ir μg/g	Pt μg/g	Au μg/g	P mg/g	S mg/g
Guanaco	14	5.08	44.3	93	44.7	71	14.6		0.26	<36	0.013	0.8	1.194		
Tombigbee R.	10	5.25	41.8	86	40.6	62.5	16.8		0.20	<30	0.007	0.7	1.281	18	<1
Bellsbank	12	5.30	45.0	87	37.6	53.9	17.4		0.15	<30	0.117	1.9	1.328	21	~1
Twannberg	16	5.20	44.6	86	37.6	51.4	17.8	163	0.13	<20	0.092	1.1	1.364	20	0.1
La Primitiva	13	5.35	46.4	94	34.5	38.6	19.9		0.14	<20	0.033	1.2	1.633	17	2

Fig. 1. Photo by Henderson (1965) of a polished section of the Bellsbank iron showing typical IIG structure. Note irregular coarse schreibersite on the lower right and upper left and the lamellar schreibersite on the lower left. Dark round area on upper left is a hole, apparently mainly resulting from the loss of coarse schreibersite. Long dimension about 10 cm.

contain moderate (~15% of area) amounts of schreibersite but no troilite was observed (FeS with diameters ⩽1 mm might have been missed).

Buchwald (1975) gives detailed structural information for Bellsbank, La Primitiva and Tombigbee River (henceforth shortened to Tombigbee). All have high schreibersite contents. Modal integration of schreibersite yields P contents of 17–21 mg/g. Most IIG schreibersite occurs as massive inclusions, as illustrated for Bellsbank in Fig. 1. It seems probable that meteoroid breakup in space and during atmospheric transit resulted in preferential fracturing in regions having high contents of the brittle mineral schreibersite, and that the schreibersite contents estimated by modal integration are appreciably lower than those in the original meteoroid.

The IIG irons contain very little troilite. Buchwald observed no FeS in the Washington or London specimens of Bellsbank but noted that a 10-mm nodule in a S. African section photographed by Groeneveld (1959) appears to be FeS. We examined this photo and think it equally likely that the irregularly circular region is a rough-textured fracture of schreibersite, possibly produced during sawing. In La Primitiva Buchwald (1975) estimates a S content of 2 mg/g; troilite in this meteorite occurs as 10- to 20-mm "nodules surrounded at some distance by rosette-schreibersite". As discussed by Wasson et al. (2007), such rosette arrangements of FeS surrounded by schreibersite and metal almost certainly reflect the presence of trapped melt. Buchwald also observed FeS in La Primitiva "as scattered spherules, ranging from 50 μm to 5 mm in diameter" and as "islands around the larger (FeS) nodules but inside the rosette-schreibersite". Buchwald (1975) did not observe FeS nodules in Tombigbee; instead, he found 10–400 μm blebs associated with the large schreibersite crystals.

In Table 1 we list rough estimates of the S contents of the four well-studied IIG irons. The La Primitiva estimate is from Buchwald (1975) and the Twannberg estimate is from Hofmann et al. (2009). Our Bellsbank and Tombigbee estimates are based on the descriptive material in Buchwald (1975).

3.2. Compositional data

Table 1 lists mean INAA data for 13 elements as well as P data from Buchwald (1975) and Hofmann et al. (2009) and S data from various sources discussed above. Only one well determined (by RNAA) Sb concentration was available but less precise INAA values are similar. As noted above, we also determine Fe but use it to correct for geometric effects or for the presence of appreciable amounts on non-metallic inclusions. To facilitate locating meteorites in the diagrams we list the mean compositions of the irons in order of increasing Au concentration in Table 1. Individual analyses are listed alphabetically in Table A1 in the Appendix together with the irradiation dates.

Metal compositions for IIG irons are plotted on log element–log Au scatter diagrams in Figs. 2 and 3.

4. THE HIGH P CONTENT OF IIG IRONS; EVIDENCE THAT SCHREIBERSITE WAS A LIQUIDUS PHASE

The IIG irons, with bulk P contents of 17–21 mg/g (Table 1), have three of the four highest P contents among the 480 irons described by Buchwald (1975); only the ungrouped iron Soper, at 21 mg/g, has a similarly high concentration. The next highest concentration reported by Buchwald is 10 mg/g in the high-Au, high-Ni, low-Ir IIIAB iron Narraburra. Most (98–99%) of the P in IIG and other iron meteorites is present as schreibersite, $(Fe,Ni)_3P$.

As noted above, in IIG meteorites the schreibersite occurs in three morphologies: coarse, lamellar and rhabditic or microprismatic. It is clear from the textures that the coarse schreibersite formed earliest, and that the lamellar and rhabditic schreibersite exsolved from the kamacite at relatively low temperatures, far below the liquidus. Hofmann et al. (2009) report mean compositions (in mg/g) for the three morphologies of schreibersite in IIG Twannberg: coarse (151 P, 105 Ni), lamellar (145 P, 172 Ni), and rhabditic (154 P, 239 Ni). These compositions show that the mass fraction of Ni in the schreibersite increased by a factor of 2.3 during the cooling history of Twannberg. Similar data for other iron meteorites were reported by Clarke and Goldstein (1978). Because the reported data are averages, the actual range must be somewhat higher. This tendency of Ni contents to increase with decreasing temperature will play an important role in our later discussion of Ni in IIG metal.

The discussion in Hofmann et al. implies that most (>90%) of the IIG P is in the coarse schreibersite. From the above ranges of bulk P contents and a mean schreibersite P content of 151 mg/g we can calculate that IIG meteorites consist of 110–140 mg/g schreibersite and, by difference, 890–860 mg/g kamacite.

During fractional crystallization of metallic magmas, P concentrates in the liquid relative to the solid. Chabot and Drake (2000) concluded that D (the solid/liquid distribution ratio) is ⩽0.12 for magmas with S contents <115 mg/g, close to the S content estimated by Wasson et al. (2007) for the evolved IIAB magma. Wasson and Huber (2006) noted that P is more incompatible than Au or As

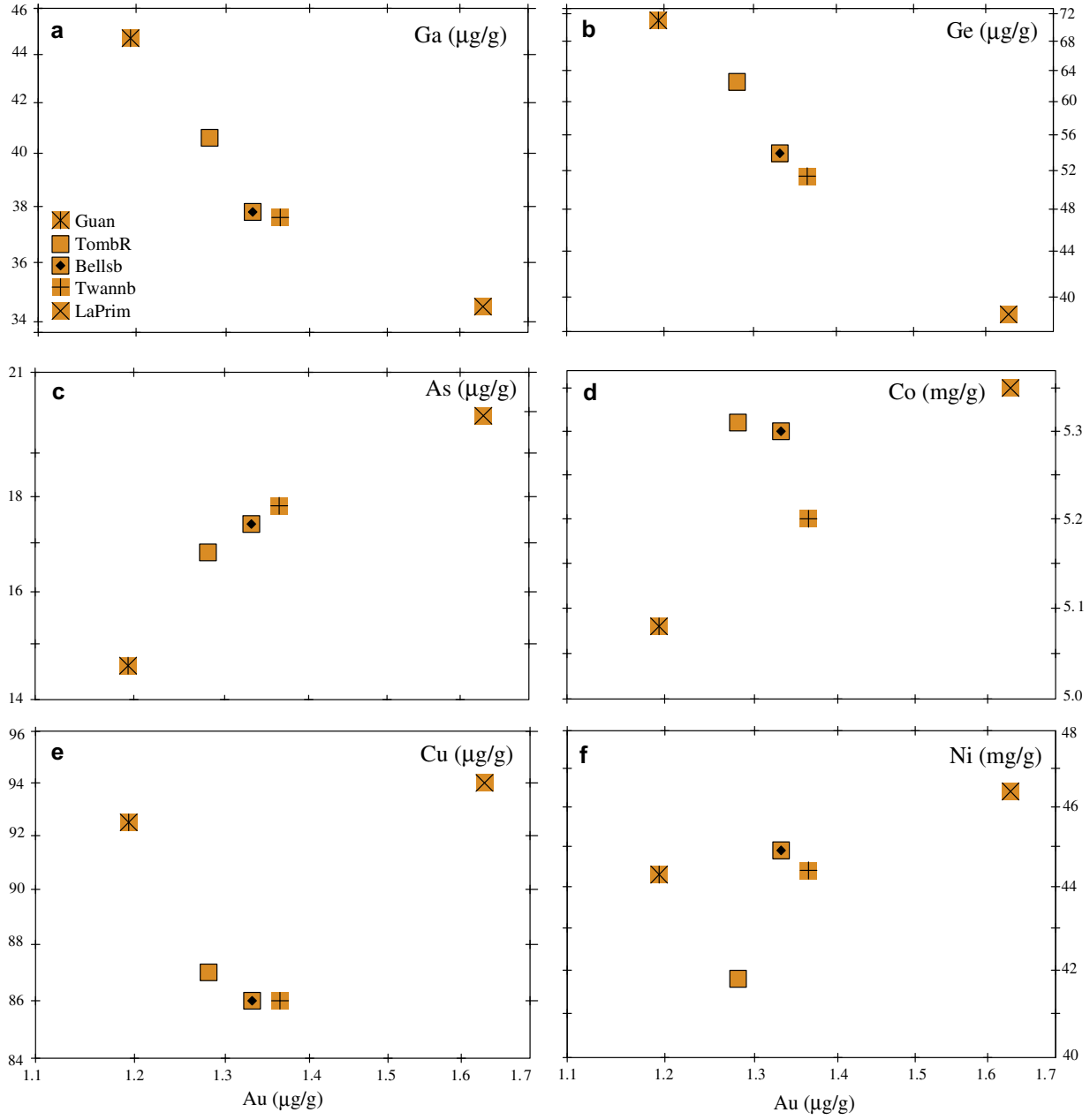

Fig. 2. Log element–log Au diagram showing IIG trends for As and five taxonomic elements that commonly show small ranges within magmatic groups; meteorites identified by abbreviations in diagram a. (a and b) Ga and Ge show smoothly descending trends with the Ge decrease a factor of 1.8, much larger than in most magmatic groups. (c) As is positively correlated with Au and, like it, shows a range of 1.4. (d) The Co range is very small, a factor of 1.04. (e and f) Ranges for Cu and Ni are small (~1.1); the scatter reflects sampling errors.

in group IID, and this appears to be the general case for magmatic groups. The high P contents may result in higher D_P values. We suggest that the D_P value when the IIG irons were crystallizing was in the range 0.10–0.20.

Clarke and Goldstein (1978) discussed the distribution of P in Bellsbank. In kamacite at the border with schreibersite they observed P concentrations as low as 0.5 mg/g and Ni concentrations as low as 16 mg/g. They observed Ni concentrations as high as 320 mg/g in rhabdites. Kamacite is clear (rhabdite-free) in 400-μm zones outside lamellar or coarse schreibersite.

5. ELEMENT-AU TRENDS IN GROUP IIG

Element-Au trends in IIG for incompatible or intermediate elements (those showing positive trends or small ranges) and for Ga and Ge (that show small ranges in most groups) are similar to those observed in magmatic groups (Fig. 2). Although some fields do not show well-defined trends, if one allows for 5% uncertainties all data could easily be fit by straight lines.

The element-Au distributions for some of the compatible elements are more complex (Fig. 3). The W and Pt data

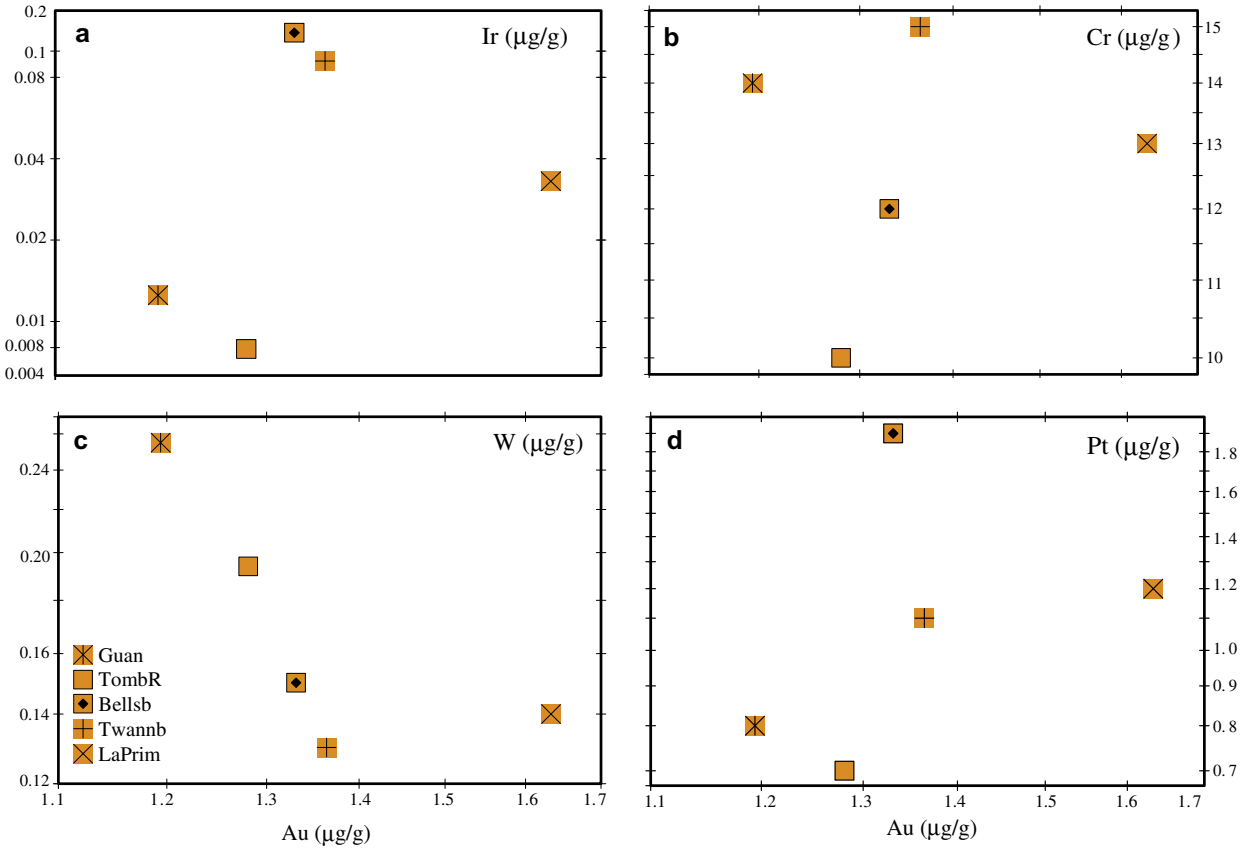

Fig. 3. Log element–log Au diagram showing IIG trends for four elements; meteorites identified by abbreviations in diagram a. (a) The Ir data scatter, with very low values in Guanaco and Tombigbee but a 20× higher value in Bellsbank followed by a decreasing trend to La Primitiva. (b) The Cr data scatter but the total range is small, 1.5. (c) The W range is small (~2) and the smooth trend may be fortuitous considering the high uncertainties of the data. d) The Pt range is also small (~2); the scatter may mainly reflect the large errors in Pt data.

are near our detection limits, thus the scatter visible on the Pt-Au diagram may be of analytical origin and the smoothly negative trend on the W-Au plot may be fortuitous. Although Cr shows apparent scatter, the total range is surprisingly small considering that some, perhaps most, Cr is in minor non-metallic phases that could result in sampling errors.

The most precise data are for Ir, Au and Co and it is interesting that the Ir–Au trend is ambiguous; it does not show the negative Ir–Au trend characteristic of all large groups, magmatic and non-magmatic. The two low-Au points (Guanaco, Tombigbee) have low-Ir contents but the Ir contents of the next two irons (Bellsbank, Twannberg) are an order of magnitude higher. These two and the high-Au IIG iron (La Primitiva) together do form a negative trend.

6. INTERRELATIONSHIP BETWEEN IIG AND IIAB IRONS

6.1. Comparison of IIAB and IIG compositional data

For most of the elements in our data set the IIG irons plot on or close to an extension of the IIAB arrays based on the Wasson et al. (2007) data set. In Figs. 4 and 5 we show the two sets together on element-Au diagrams (and arranged in the same order as in Figs. 2 and 3). In this subsection we note the differences and similarities in the two groups. In the next subsection we present a model.

The first thing to note is that the Au values in 4 of the 5 IIG irons overlap those in the four IIAB irons having the highest Au values (the evolved IIAB quartet consisting of Santa Luzia, Sao Juliao, Silver Bell and Summit). Because Au is well determined and almost entirely in metal, it is important to compare IIG compositions with the most evolved IIAB irons and especially with this cluster of four IIABs that are separated from the remainder of the group by a small hiatus in Au concentration. A complication is that Wasson et al. (2007) modeled the members of the evolved quartet as equilibrium mixtures of metal with 50–70 wt% trapped melt.

Six elements are plotted against Au in Fig. 4. Five of these elements (all except As and Au) have served as taxonomic elements in the past, i.e., they have been found to show limited intragroup ranges that differ from group to group. On Fig. 4 two of these elements (Ni and Ge) show dramatic offsets between the IIAB evolved quartet and the IIG irons. Gallium shows a sharply decreasing trend in IIB but Guanaco, at the low-Au extreme, has a Ga content similar to three members of the IIAB quartet. In the

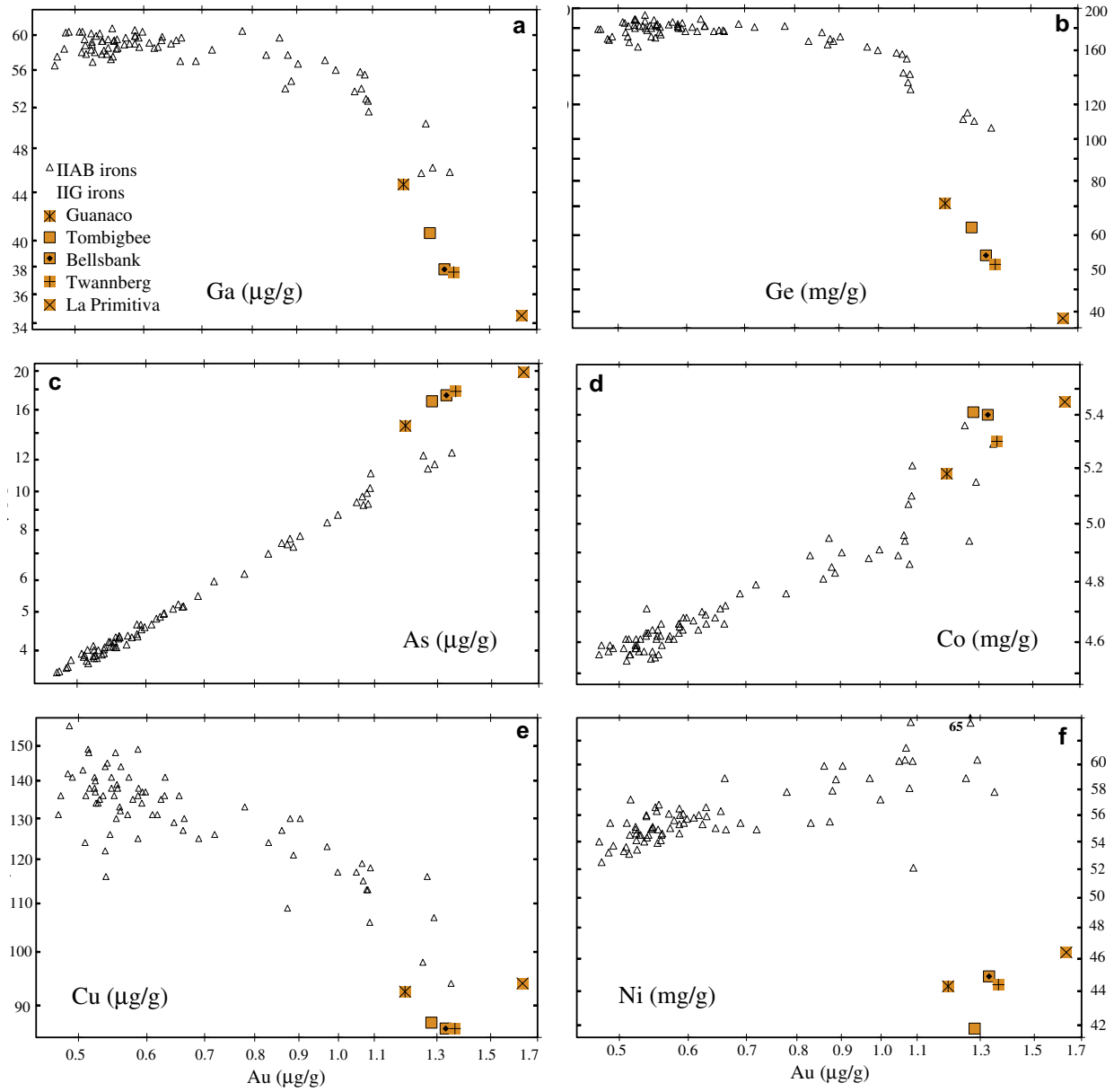

Fig. 4. Log element–log Au diagram showing both IIAB and IIG trends for As and five taxonomic elements in metal samples; with the exception of Ni, the IIG fields plot close to extrapolation of the IIAB fields. Gallium (a), Ge (b) and Cu (e) plot 5–30% lower than a rough extrapolation of the IIAB trend, IIG As (c) plots 30% above the IIAB trend and Co on the high edge of the trend. The most striking separation is for Ni, but much of the bulk Ni in IIG is in the schreibersite, and Ni strongly prefers schreibersite to kamacite at low temperatures.

past a close genetic link between IIG and IIAB has been rejected largely on the basis of the 10–30% lower concentrations of Ga, Ge and Ni in IIG irons relative to the evolved IIAB irons.

The total IIAB range in Ga (Fig. 4a) is a factor of ~1.3 and the apparent offset (at a Au value of 1.3 µg/g) in IIG is downwards by a factor of 1.1 below the IIAB trend. The Ge offset (Fig. 4b) is larger (a factor of 1.3) than that of Ga, and it is probably not coincidental that the Ge range in IIAB is a factor of 1.8, appreciably larger than that of Ga. Both elements become compatible at Au concentrations >0.9 µg/g but D_{Ge} is increasing faster than D_{Ga}.

The precisely determined element Co shows a continuum between IIAB and IIG with no offset. Note that the total range across the two groups is small, a factor of 1.2. The group-IIG trend is well-defined and two IIG members are unresolvable from two of the evolved IIAB quartet.

Especially interesting is As (Fig. 4c) which is also a precisely determined element. Here the trend in IIG has a similar slope to that in IIAB but the IIG As points plot about 1.4× higher than the IIAB trend. As discussed below, this may reflect exsolution from schreibersite.

In contrast, the compatible elements in IIG irons consistently lie on or close to an extrapolation of the trends in

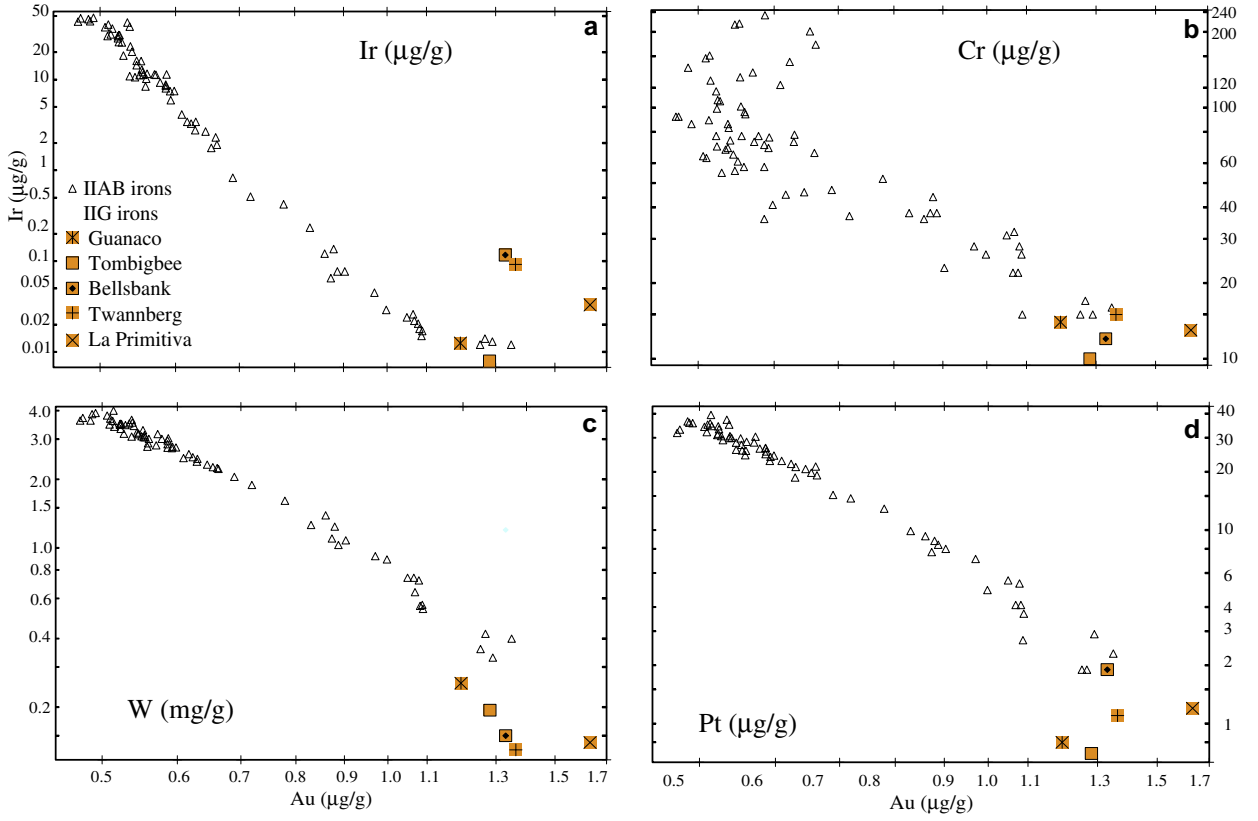

Fig. 5. Log element–log Au diagram showing both IIAB and IIG trends for four compatible elements. (a) Three IIG Ir points plot above the IIAB trend but the other two Ir points and all data for Cr (b), W (c) and Pt (d) plot on or just below the IIAB trend. The close relationship between IIG and IIAB irons shown here and in Fig. 4 suggests that the two groups formed from a common magma.

IIAB irons (Fig. 5). Two of the points on the Ir–Au diagram (Fig. 5a) plot within the IIAB trend whereas the other three plot an order of magnitude above the trend. The IIG Cr data (Fig. 5b) plot along an extension of the IIAB trend; Cr data tend to scatter because much of the element is in minor phases such as daubreelite, but such effects are not recognizable in these data. Most of the W (Fig. 5c) and Pt (Fig. 5d) data plot 1.5–2× lower than the IIAB trend but La Primitiva at the high-Au extreme plots near the extension of the trend on each diagram and Bellsbank plots among the IIAB evolved quartet. Because of large uncertainties in the IIG W and Pt data one can only conclude that apparent IIG–IIAB differences are small.

We know of only one other example of two groups that are as closely related as IIAB and IIG; the members of the small, C-rich IIIE group are only marginally resolvable from the IIIAB irons (Malvin et al., 1984; Wasson et al., 1998) and it is possible that they may have formed on the same asteroid. The close compositional relationship between IIG and IIAB provides strong evidence of a genetic link. There are some features that are slightly anomalous such as the high-Ir contents of the three high Au IIG irons, but such anomalies are found in all large groups and can usually be rationalized by stochastically occurring processes such as melt trapping and contamination from earlier formed metal. In the remainder of this paper we will examine the possibility that IIG irons could have formed from a highly evolved IIAB magma.

6.2. Role of schreibersite in determining the composition of IIG metal

The schreibersite abundance is high in IIG irons. For those elements that have schreibersite/metal partition ratios that are large and temperature dependent, metal compositional data may give a misleading picture of the composition of the parental magma. For such elements one cannot follow the common practice of using estimates of metal/melt partition ratios to infer the composition of the parental magma. It appears to us that metal/schreibersite partitioning played an important role in determining the Ni and As concentrations in IIB metal and may have played a role in determining metal concentrations for other elements.

Much of what follows depends on assumptions which we have attempted to state explicitly. An important assumption, and one that we will question late in the section, is that, for the high-Au IIAB irons and the full range of IIG irons, Au concentration increased monotonically as the evolution of the IIAB magma proceeded. It is important, however, to note that Wasson et al. (2007) interpreted the evolved quartet of IIAB irons as having formed from mixes of solid metal with 50–70 wt% of trapped melt. Because the solid/liquid distribution coefficient for Au, D_{Au}, is low (~0.6), large amounts of trapped melt result in moderately large increases in Au concentrations.

In Section 4 we calculated that the mean schreibersite content of IIG irons is in the range 110–140 mg/g. In Section 3 we noted that, because fracturing in space and during atmospheric passage preferentially occurred in schreibersite-rich regions, the actual abundance of schreibersite must have been somewhat larger, perhaps 200 mg/g or larger.

The relevant distance is that over which diffusional equilibration of metal was able to occur. Based on the gradients observed in the IIIAB Cape York Agpalilik trapped-melt-rich iron by Esbensen et al. (1982), this distance was at least several tens of centimeters but less than a meter. We suggest, over this scale, the abundance of schreibersite in the final IIG magma pockets was $\geqslant$200 mg/g. As discussed in the next section, the last liquid to solidify may have reached the composition of the Fe–P eutectic in which the schreibersite mass fraction is 567 mg/g (Raghavan, 1988).

In Section 4 we noted that the mean Ni content of IIG schreibersite ranges from 105 mg/g in coarse schreibersite to 239 mg/g in rhabdites. This seems to primarily reflect differences in the mean temperature recorded by the schreibersite and secondarily the Ni content of the metal with which the schreibersite is communicating. There is no reason to doubt that the Ni content of the coarse schreibersite was appreciably lower when it formed, probably (as discussed in the following section) mostly at a temperature near that of the Fe–P eutectic, about 1320 K.

We do not know of Ni schreibersite/metal partitioning data at this temperature. However, it seems highly probable that the partition ratio is much nearer to unity than that calculated relative to the coarse schreibersite. The comparison should be in terms of the atom ratio Ni/(Fe + Ni) for the two phases; we will call this ratio N. We can use our data and that of Hofmann et al. (2009) to calculate that the N_{schr}/N_{met} ratio was ~6.3 at the temperature at which the rhabdites equilibrated. To calculate the ratios at the higher temperatures at which the lamellar and coarse schreibersite compositions were established we must estimate the Ni contents of the kamacite; these values will be intermediate between those of the present metal (~44 mg/g) and those of the metal when the last melt crystallized. We list rough estimates of these interpolated metal compositions in Table 2.

To estimate the metal concentrations we assume that the initial Ni content of the IIG metal was the same as that of the metal in the evolved IIAB quartet, about 60 mg/g. We then use a rough interpolation to estimate the Ni content of the metal when the composition of the lamellar and massive schreibersite stopped equilibrating with the metal. From these metal and schreibersite compositions we estimated the N_{schr}/N_{met} ratios. The schreibersite was assumed to consist only of Fe, Ni and P with the P content 152 mg/g at all temperatures. We assumed that the Ni and Fe concentrations in the metal totaled 990 mg/g. We then estimated a Ni content of the schreibersite at the eutectic temperature that would give us a D value greater than but close to unity (and much less than the value of 2.7 calculated in Table 2 for the temperature at which the massive schreibersite stopped equilibrating with the metal).

We constructed a mass-balance model to determine what fraction of schreibersite would be required to explain the Ni content in IIG metal by the gradual transfer of Ni from the initial value (60 mg/g) in the metal to produce our estimated Ni content of schreibersite. The results of this crude calculation of schreibersite Ni values are listed in Table 2. We found that the assumed eutectic Ni content of schreibersite could be obtained if the initial fraction of schreibersite was 240 mg/g. This high schreibersite content seems possible if, as suggested earlier, schreibersite-rich regions were selectively destroyed in space or during atmospheric passage.

Our suggested explanation of the high As content of IIG metal is that As entered schreibersite at high temperatures and exsolved and transferred into the metal at low temperatures. Because As is a congener of P, it seems reasonable that, at temperatures near that of the Fe–P eutectic (when P crystalline sites are larger and more accommodating of As), the As/P ratio in schreibersite might be approximately that in the magma. Our modeling of the IIAB magma (shown in Ir–As diagrams in Wasson et al., 2007) yields As concentrations in the magma at the time of formation of the evolved IIAB quartet of ~15 μg/g. As noted earlier, at this point the P content of the magma was probably about 60 mg/g; thus, the As/P mass ratio was $\sim 2.5 \times 10^{-4}$ (continued evolution towards the eutectic would not have changed this ratio). If we assume the same ratio in the massive schreibersite that formed at the eutectic temperature, from the mean P content of the schreibersite we calculate an As concentration of 37.5 μg/g. Wasson et al. (2007) report an As content in a sample mainly consisting of schreibersite from the IIAB iron Santa Luzia of 1.9 μg/g; thus, most As that (hypothetically) entered schreibersite at high temperatures transfers back into the metal at low temperatures. From Fig. 4 we can estimate that the excess As in IIG metal relative to IIAB metal is about 5 μg/g. The rough model given here provides ~35 μg/g As for every gram of schreibersite and can thus account for 5 μg/g As excess with about 130–140 mg/g schreibersite, similar to that observed in IIG irons.

The other large offset in our IIAB–IIG comparison is observed for Ge. Based on a distribution ratio is <1 at both high and low temperatures. On the other hand, we think the offset may be related to the very low-S content of the IIG irons. Because the solubility of S in metal is so low, almost all the observed S is the result of trapped melt. The IIG irons seemed to have trapped almost none of the S-rich melt

Table 2
Measured Ni concentrations in schreibersite (Hofmann et al., 2009) and metal (in bold), estimated compositions of eutectic schreibersite and of metal compositions in equilibrium with the various forms of schreibersite (in italics) and calculated Ni schreibersite/metal distribution ratios (Ns/m). Units of sch Ni and met Ni are mg/g. See text for details.

Schreibersite	Sch Ni	Ni/ Fe + Ni	Met Ni	Ni/ Fe + Ni	Ns/ m
Rhabdite	**239**	0.282	**44**	0.0444	6.3
Lamellar	**172**	0.203	*45*	0.0455	4.5
Coarse	**105**	0.124	*46*	0.0465	2.7
Eutectic	*56*	0.066	*60*	0.0606	1.1

formed during this crystallization stage; their observed S contents probably reflect the trapping of small amounts of P-rich melt. We suggest that Ge preferentially entered the S-rich melt that formed during IIG crystallization, and that this melt was largely lost from the various systems that produced the IIG irons. We will define a S-rich melt/P-rich melt ratio $D_{SL/PL}$ that would need to be $\geqslant 2$ to make an appreciable change in the composition of the P-rich melt. If this interpretation of the Ge offset is correct, the model may also account for the smaller downward offsets in Ga, Cu, W and Pt. We will discuss the physical aspects of this model in the following section.

The discussion until now has been based on the assumption that the Au content of a magma increases monotonically during crystallization and our discussion of offsets and their origins is based on a corollary of this assumption, that the Au content of IIG and IIAB irons provides an approximate measure of the degree of crystallization of the magma. However, according to Wasson et al. (2007), the evolved IIAB quartet consist of equilibrium mixes of metallic solids and large amounts of trapped melt; according to their model several irons (e.g., Derrick Peak 78009 and Lake Murray) experienced similar degrees of crystallization as the evolved quartet but had much lower degrees of trapped melt and thus lower Au contents.

A possibility that we cannot rule out is that $D_{SL/PL}$ is >1 for Au, with the result that the IIG Au values may have been driven to lower values. Examination of Figs. 4 and 5 shows that, if IIG Au concentrations were increased about 20%, most of the offsets for elements other than Ni (and 3 Ir values) would become smaller and perhaps not resolvable. This scenario leads to the conclusion that the IIG irons are from a more evolved liquid than the evolved IIAB quartet, which (at least for the well-studied iron Santa Luzia) seems to have retained most of the S-rich liquid that formed as it crystallized. We will return to these points in our summary.

7. POSSIBLE FORMATION OF MASSIVE SCHREIBERSITE AND IIG IRONS IN THE IIAB CORE

7.1. Formation of massive schreibersite in the IIAB core

In our opinion, the irregular textures of the coarse schreibersite inclusions in IIG irons seem best understood in terms of crystallization as a liquidus phase. This contrasts with the interpretation of Clarke and Goldstein (1978), who adopted the view that the coarse schreibersite in iron meteorites resulted from homogeneous nucleation of schreibersite within metal followed by solid-state exsolution of P from the metal.

Wasson et al. (2007) refuted this interpretation based on common occurrences of schreibersite in the evolved IIAB irons, particularly Santa Luzia; they showed that the rosette arrangement of interior FeS and exterior schreibersite is exactly that expected from the crystallization of a pocket of trapped melt. Schreibersite crystallized first on the walls of the fluid-filled region. The metal-FeS eutectic was the last liquid to crystallize, commonly (but not always) near the center of the original melt pocket.

In either of these models, the volume of the coarse schreibersite continued to expand as the metal cooled from the schreibersite nucleation temperature (ca. 1320 K) down to the temperature at which the diffusion of P through the metal became so slow that lamellar schreibersite nucleated.

In the IIG irons schreibersite is more abundant and troilite much less abundant than in Santa Luzia and the other members of the evolved quartet; thus, the formation processes differed, at least in detail. Two relevant issues are (a) the reason for the low FeS abundances and (b) the conditions necessary to make schreibersite a liquidus phase.

A relevant fact is that, because of the low solubility of S in Fe–Ni phases, the presence of coarse FeS is always an indication of trapped melt. When large amounts of FeS and schreibersite are together it is reasonable to use their relative abundances to estimate the P/S ratio in the parental liquid. It is based on such estimates that Wasson et al. (2007) concluded that the P/S ratio in in the initial IIAB magma was about 0.25, similar to the ratio estimated by Wasson (1999) for the initial IIIAB magma.

The evolution of the IIAB core can be discussed in terms of the liquid immiscibility Fe–S–P diagram given by Wasson et al. (2007; Fig. 10). In the IIAB core the P/S ratio was probably still ~0.25 at the onset of liquid immiscibility; at this point the fraction of the S-rich liquid was very small and the P-rich liquid had the composition of the residual magma. However, by the time Santa Luzia crystallized the amount of the S-rich phase had increased and the P/S ratio was ~0.54 (Wasson et al., 2007).

To put some perspective in the discussion, we have copied a portion of the Fe–P phase diagram (Raghavan, 1988) as Fig. 6. This shows that the system crystallizes as a eutectic at a temperature of 1321 K; the P content of the eutectic is 101 mg/g. Thus, to reach the eutectic, crystallization of additional metal must occur following immiscibility. Note

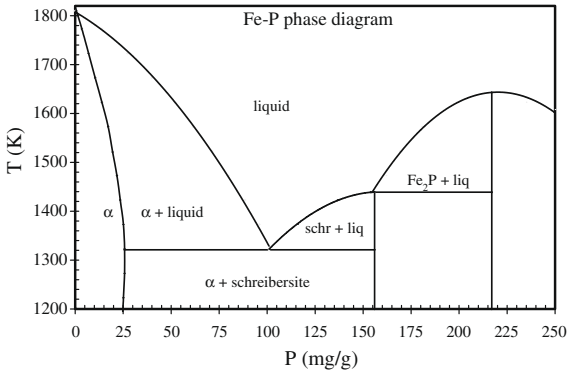

Fig. 6. Portion of Fe–P phase diagram (after Raghavan, 1988). This phase diagram should approximate that of the evolved IIAB P-rich liquid in which the S/P wt ratio is <1 and P concentrations >50 mg/g. A small γ-iron field extending from 1200 to 1650 K at P<10 mg/g is not shown and not relevant for this discussion. In the IIAB and IIG core(s) schreibersite becomes a liquidus phase at the eutectic temperature of ~1320 K.

that the P content of the crystallizing α-iron reaches a maximum of ~26 mg/g near the eutectic temperature.

A reasonable working estimate is that the P/S ratio in the P-rich magma was around unity when the IIG irons started to form, perhaps containing ~40 mg/g of each element. The more extensive phase diagrams of Schürmann and Neubert (1980) and Raghavan (1988) indicate that the S content of the P-rich liquid had fallen to 10–15 mg/g when the liquid reached the Fe–P eutectic at ~100 mg/g P.

7.2. Final evolution of the IIAB magma

According to the Fe–S–P phase diagram given in Fig. 10 of Wasson et al. (2007), the temperature of the IIAB magma was ~1520 K at the onset of liquid immiscibility. Fig. 6 shows that the temperature was about 1320 when the Fe–P eutectic crystallized. The viscosity of the magma increased both with decreasing temperature and with increasing P content. We suggest that this increase in viscosity played an important role in the formation of the IIG irons. In particular, we suggest that the morphology of the liquid–solid interface became more and more irregular and dendritic as the temperature approached the eutectic minimum.

We picture that the metal formed irregular cusps and cavities and that the liquids in these cavities were not included in the convective motions of the overlying magma. As temperatures continued to fall, these cavities became more and more isolated. We suggest that these cavities were filled with the trapped melt that became the IIG irons.

The IIG irons have very low contents of FeS and, as discussed above, we suspect that some of the compositional differences between the IIG irons and the evolved quartet of IIAB irons is that the former lost nearly all of the S-rich immiscible melt as it formed whereas the latter retained much of this melt. For this reason there must have been passages through which most of the more-buoyant S-rich melt could escape out the top of the hypothetical IIG cavities. By the time temperatures had fallen to the eutectic temperature, the solubility of S in the final melt was probably very low, 10–15 mg/g.

Another related scenario is that the trapped melt regions were closed systems but were much larger than subsolidus diffusion lengths (~0.5 m). In this case the S-rich melt might have collected at the top of the chamber. After solidifying, elements such as Au or Ge that may have selectively partitioned into this melt would have entered the metal but not have been able to diffuse back to the P-rich locations where IIG irons formed.

This model requires that our meteorite sample set does not include these FeS-rich, metal-poor regions. According to Ulff-Møller (1998) the S-rich melt had a S content of 310–320 mg/g, similar to the S content of the Fe–S eutectic. After solidification such a melt contains only 8.6 vol% metal. It has been repeatedly recognized (e.g., Kracher and Wasson, 1982) that FeS-rich meteorites are incompletely represented among meteorites, probably because of attrition in space and during atmospheric passage related to the low strength and low resistance to shear of FeS.

7.3. Were the IIG irons formed in the IIAB core?

We think it is probable that the schreibersite-rich IIG irons formed in the IIAB core. The fact that, on the ten log-element, log-Au diagrams of Figs. 4 and 5, the IIG irons consistently plot close to an extension of the IIAB fields is the strongest evidence. The case is strengthened by the fact that plausible processes can explain most and possibly all of the small offsets observed for some of the elements. The largest of these offsets is for Ni, and there is no doubt that some and perhaps all of the difference reflects the solid-state redistribution of Ni between kamacite and schreibersite. The Ni/(Ni + Fe) ratio in coarse schreibersite is 2.3 times lower than that in rhabditic schreibersite, and this ratio was probably 1.5 to 2× lower in the coarse schreibersite that initially formed at the eutectic temperature.

More data are needed to confirm the IIAB–IIG relationship. Oxygen isotopic data would be telling, but oxides are very rare and there are still no O-isotope data on any of the IIAB or IIG irons. Germanium isotopes (Luais, 2007) in IIAB irons show compositional offsets that may prove useful for testing some of the processes here discussed.

8. SUMMARY

The IIG irons are hexahedrites containing high amounts of coarse schreibersite; they are the most P-rich iron meteorites with only one other iron (Soper) having a similarly high content of P. Studies of the five members of the magmatic iron meteorite group IIG show trends roughly similar to irons formed by the fractional crystallization of a magma. On element-Au diagrams they show small ranges in Ni and Co and relatively small ranges and smooth trends on plots of As, Ga and Ge with the Ge range being slightly higher than in most magmatic groups (factor of 1.3). For other elements trends are generally consistent with fractional crystallization with some scatter resulting from experimental error. Stochastic variations in the abundance of minor or trace phases are probably responsible for the scatter on the Cu, Ir and Cr diagrams.

When the IIG data are plotted together with the IIAB irons on element-Au diagrams it is found that the IIG irons always plot near the high-Au end of the IIAB field suggesting that the two groups formed in the same asteroidal core. In some cases such as Co the IIG irons plot directly along an extrapolation of IIAB trends; in others there are small (by factors $\leqslant$1.6) positive or negative offets relative to the extrapolated trend.

At the evolved (high-Au) end of the IIAB set are four irons that we call the "evolved IIAB quartet". Wasson et al. (2007) showed that the compositional data implied that these four irons have large fractions (50–70%) of trapped melt. These authors also echoed the opinion expressed in earlier papers that the IIAB magma experienced liquid immiscibility during its evolution.

We suggest that, like the IIAB evolved quartet, the IIG irons incorporated a large fraction of trapped melt, and that the compositional differences between them and the IIAB evolved quartet mainly reflect details in their final evolution. In particular, the IIAB evolved quartet seems

to have retained a large fraction of both the S-rich and P-rich melts that were trapped whereas the IIG irons lost almost all of the late-formed S-rich melt. The latter process is not only responsible for the low-S contents of the IIG irons, it would also have depleted them in elements that strongly partition into the S-rich melt (Ge may be an example). We speculate that this could be the reason that some elements have lower concentrations in IIG irons relative to trends expected from group IIAB.

The most striking compositional difference between the IIAB quartet and the IIG irons is in terms of Ni. It was discussed by Clarke and Goldstein (1978) and recently confirmed by Hofmann et al. (2009), the Ni content of the coarse schreibersite in IIG irons is about 2.3× lower than that in the rhabditic schreibersite that exsolved from the metal at low temperatures. We suggest that the low Ni content of IIG metal can largely be accounted for by diffusive transport of Ni out of the metal into the coarse schreibersite (which accounts for >90% of the schreibersite in IIG) as the irons slowly cooled from the eutectic temperature. We speculate that the Ni/(Ni + Fe) ratio in the schreibersite that formed at eutectic temperatures was much lower than that now found in the coarse schreibersite, and we show that Fe–Ni exchange can account for the observed difference.

Our main approach to explain the remaining compositional offsets between IIAB and IIG was to assume that Au was not strongly affected by the processes responsible for the differences between the two groups, and to suggest processes such as gradual exsolution from schreibersite (for As) or gradual extraction by escaping S-rich melt (for Ge and some other elements) could account for the differences.

However, if the latter process was effective at extracting Au into the escaping S-rich melt, it could explain most of the differences between the placement of IIG irons relative to the IIAB trends. Key research for the future is to carry out experiments to assess the partitioning of siderophiles (and especially Au and Ge) between immiscible S-rich and P-rich melts.

ACKNOWLEDGMENTS

We thank Beda Hofmann for stimulating this reexamination of IIG trends, Heinz Huber for assistance in gathering the INAA data, and Nancy Chabot for discussions. Useful and constructive reviews were provided by Misha Petaev, Catherine Corrigan and Dave Cook. We are grateful to Tram Le for assistance with the construction of the diagrams. A number of curators provided samples. This research was largely supported by NASA Grant NNG06GG35G.

APPENDIX A

In Table A1 we list the data for replicate samples of the IIG irons. The year and month of the irradiation are given in the second column. The four Sb analyses are the only INAA concentrations having ⩽15% uncertainties.

With rare exceptions the analyses made in 1986 and later were given twice as much weight as the earlier analyses in the means. A few indicated values having high uncertainties were either not included or given less weight in the means listed in Table 1. Note that one analysis of La Primitiva was based on a sample originally designated Tarapaca and that three different specimens of Twannberg were studied.

Table A1
Alphabetical list of replicate INAA data for IIG irons.

Meteorite	Date yymm	Cr μg/g	Co mg/g	Ni mg/g	Cu μg/g	Ga μg/g	As μg/g	Sb[§] μg/g	W μg/g	Re ng/g	Ir μg/g	Pt μg/g	Au μg/g
Bellsbank	8205	13	5.32	39.2	39	40.0	18.3		<0.29	<90	0.111		[*]1.580
Bellsbank	8212	<24	[*]4.97	52.7	96	38.0	16.9	130	<0.31	<66	0.090		1.350
Bellsbank	0112	11	5.32	41.4	83	38.0	17.9		0.14	<40	0.129	[*]2.7	1.372
Bellsbank	0307	14	5.26	53.4	83	35.1	16.7		0.16	<25	0.122	1.5	1.272
Guanaco	0101	16	5.06	44.7	94	45.6	14.9		0.26	<47	0.010	0.8	1.210
Guanaco	0105	12	5.10	43.8	91	43.7	14.2		0.25	<36	0.015	0.8	1.177
La Primitiva	9103	13	5.26	47.0	97	33.7	19.8		0.10	<40	0.035	0.8	1.689
La Primitiva	9104	13	5.31	48.8	94	34.6	19.6		0.14	<24	0.039	1.8	1.635
La Prim. (Tarapaca)	0809	03	5.48	43.4	92	35.3	20.3		[†]0.23	<38	0.026	1.2	1.517
Tombigbee River	8210	8	5.25	40.5	83	41.1	17.7		<0.18	<90	0.0092		1.315
Tombigbee River	8212	<13	5.15	45.1	90	42.8	17.5		0.23	<28	<.023		1.410
Tombigbee River	0112	9	5.31	37.8	85	40.9	16.4		0.16	<40	0.0055		1.283
Tombigbee River	0307	13	5.53	42.6	89	40.4	16.4		0.21	<35	0.0090	0.7	1.279
Twannberg I	8605	14	5.18	43.7	94	38.8	18.6		[*]0.72	<26	0.087	<1.5	1.321
Twannberg I	8606	13	5.25	44.7	85	37.0	17.3		0.19	<24	0.085	<1.4	1.379
Twannberg I	0809	13	5.14	44.1	82	37.8	17.5		0.10	<30	0.082	1.3	1.318
Twannberg II	0107	14	5.17	46.7	89	37.3	18.0	140	0.11	<30	0.101	0.9	1.406
Twannberg II	0112	19	5.27	43.3	89	39.5	18.2	160	0.16	<40	0.101	[*]3.3	1.407
Twannberg III	0809	14	5.18	43.7	75	35.2	16.9	180	0.09	<30	0.098	1.0	1.351

[*] Value not included in mean.
[†] Value given reduced weight in mean.
[§] INAA Sb values listed only if estimated uncertainties ⩽20%.

REFERENCES

Buchwald V. F. (1975) *Handbook of Iron Meteorites*. University California Press, 1418 pp.

Chabot N. L. and Drake M. J. (2000) Crystallization of magmatic iron meteorites: The effects of phosphorus and liquid immiscibility. *Meteorit. Planet. Sci.* **35**, 807–816.

Clarke R. and Goldstein J. (1978) Schreibersite growth and its influence on the metallography of coarse-structured iron meteorites. *Smithson. Contrib. Earth Sci.* **21**, 1–80.

Esbensen K. H., Buchwald V. F., Malvin D. J. and Wasson J. T. (1982) Systematic compositional variations in the Cape York iron meteorite. *Geochim. Cosmochim. Acta* **46**, 1913–1920.

Groeneveld D. (1959) A new iron meteorite from Bellsbank, Barkly West District. *Trans. Geol. Soc. S. Africa* **62**, 75–79.

Henderson E. P. (1965) Hexahedrites. *Smithson. Misc. Coll.* **148**, 1–41.

Hofmann B. A., Lorenzetti S., Eugster O., Krähenbühl U., Herzog G., Serefiddin F., Gnos E., Eggimann M. and Wasson J. T. (2009) The Twannberg (Switzerland) IIG iron meteorites: mineralogy, chemistry, and CRE ages. *Meteorit. Planet. Sci.* **44**, 187–199.

Kracher A. and Wasson J. T. (1982) The role of S in the evolution of the parental cores of the iron meteorites. *Geochim. Cosmochim. Acta* **46**, 2419–2426.

Luais B. (2007) Isotopic fractionation of germanium in iron meteorites: significance for nebular condensation, core formation and impact processes. *Earth Planet. Sci. Lett.* **262**, 21–36.

Malvin D. J., Wang D. and Wasson J. T. (1984) Chemical classification of iron meteorities–X. Multielement studies of 43 irons, resolution of group IIIE from IIIAB, and evaluation of Cu as a taxonomic parameter. *Geochim. Cosmochim. Acta* **48**, 785–804.

Raghavan V. (1988) The Fe–P–S System. In *Ternary Systems Containing Iron and Sulphur*, pp. 209–217.

Russell S. S., Folco L., Grady M. M., Zolensky M. E., Jones R., Righter K., Zipfel J. and Grossman J. N. (2004) The Meteoritical Bulletin, no. 88, July 2004. *Meteorit. Planet. Sci.* **39**, A215–A272.

Schürmann E. and Neubert V. (1980) Schmelzgleichgewichte in den eisenreichen Ecken der Dreistoffsysteme Eisen-Schwefel-Kohlenstoff, Eisen-Schwefel-Phosphor und Eisen-Schwefel-Silicium. *Giessereiforschung* **32**, 1–5.

Scott E. R. D., Wasson J. T. and Buchwald V. F. (1973) The chemical classification of iron meteorites-VII. A reinvestigation of irons with Ge concentrations between 25 and 80 ppm. *Geochim. Cosmochim. Acta* **37**, 1957–1983.

Ulff-Møller F. (1998) Effects of liquid immiscibility on trace element fractionation in magmatic iron meteorites: a case study of group IIIAB. *Meteorit. Planet. Sci.* **33**, 207–220.

Wasson J. T. (1974) *Meteorites–Classification and Properties*. Springer, New York, 316 pp.

Wasson J. T. (1999) Trapped melt in IIIAB irons; solid/liquid elemental partitioning during the fractionation of the IIIAB magma. *Geochim. Cosmochim. Acta* **63**, 2875–2889.

Wasson J. T., Choi B.-G., Ulff-Møller F. and Jerde E. (1998) Chemical classification of iron meteorites: XII. New members of the magmatic groups. *Geochim. Cosmochim. Acta* **62**, 715–724.

Wasson J. T. and Huber H. (2006) Compositional trends among IID irons; their possible formation from the P-rich lower magma in a two-layer core. *Geochim. Cosmochim. Acta* **70**, 6153–6167.

Wasson J. T., Huber H. and Malvin D. J. (2007) Formation of IIAB iron meteorites. *Geochim. Cosmochim. Acta* **71**, 760–781.

Wasson J. T. and Kimberlin J. (1967) The chemical classification of iron meteorites - II. Irons and pallasites with germanium concentrations between 8 and 100 ppm. *Geochim. Cosmochim. Acta* **31**, 2065–2093.

Wasson J. T., Ouyang X., Wang J. and Jerde E. (1989) Chemical classification of iron meteorites: XI. Multi-element studies of 38 new irons and the high abundance of ungrouped irons from Antarctica. *Geochim. Cosmochim. Acta* **53**, 735–744.

Wasson J. T. and Richardson J. W. (2001) Fractionation trends among IVA iron meteorites: contrasts with IIIAB trends. *Geochim. Cosmochim. Acta* **65**, 951–970.

Associate editor: Richard J. Walker